




Spin order in the classical spin kagome antiferromagnet $\text{Mg}_x\text{Mn}_{4-x}(\text{OH})_6\text{Cl}_2$ Md. Mahbubur Rahman Bhuiyan ¹, Xu-Guang Zheng ^{1,2,*}, Masato Hagihala ³, Shuki Torii,³
Takashi Kamiyama,³ and Tatsuya Kawae⁴¹*Department of Physics, Graduate School of Science and Engineering, Saga University, Saga 840-8502, Japan*²*Department of Physics, Faculty of Science and Engineering, Saga University, Saga 840-8502, Japan*³*Institute of Materials Structure Science, KEK, Tokai 319-1106, Japan*⁴*Department of Applied Quantum Physics, Faculty of Engineering, Kyushu University, Fukuoka 819-0395, Japan*

(Received 27 February 2020; revised manuscript received 18 March 2020; accepted 30 March 2020; published 21 April 2020)

Geometrically frustrated kagome-lattice antiferromagnets have received much attention because of their exotic magnetic behaviors. Here we report the synthesis, structure, and magnetism of an $S = 5/2$ quasiclassical new spin kagome compound. Polycrystalline compounds of $\text{Mg}_x\text{Mn}_{4-x}(\text{OH})_6\text{Cl}_2$, with a nominal ideal chemical formula of $\text{MgMn}_3(\text{OH})_6\text{Cl}_2$, have been successfully synthesized by selectively substituting the triangular-lattice-plane Mn^{2+} with nonmagnetic Mg^{2+} . The compounds studied crystallize in rhombohedral structure in space group $R\bar{3}m$, in a similar crystal structure to the much-researched quantum spin liquid candidates herbertsmithite $\text{ZnCu}_3(\text{OH})_6\text{Cl}_2$ and tondite $\text{MgCu}_3(\text{OH})_6\text{Cl}_2$. Antiferromagnetic transition below $T_N \sim 8$ K and a 120° nearest-neighbor spin ordering confined in the kagome plane with positive spin chirality have been revealed by magnetic susceptibility measurements and neutron diffraction experiment. The obtained value of critical exponent $\beta = 0.35$ agrees with a three-dimensional Heisenberg spin model. The present work suggests the intrinsic nature of long-range order in classical Heisenberg kagome antiferromagnet and provides a classical reference system to quantum kagome antiferromagnets.

DOI: [10.1103/PhysRevB.101.134424](https://doi.org/10.1103/PhysRevB.101.134424)**I. INTRODUCTION**

Geometrically frustrated magnets have received intense attention because of the unconventional macroscopic quantum states such as spin liquids, spin ice, spin nematic, etc. [1,2]. Central in the search for exotic quantum states are kagome lattices—lattices of intersecting webs of corner-sharing triangles—that are prized for large geometric frustration and usefulness for studying the physics of frustrated magnetism, as well as correlated and topological quantum electronic states [3–8]. However, the number of real materials has been severely limited. Among them, herbertsmithite, $\text{ZnCu}_3(\text{OH})_6\text{Cl}_2$, is often discussed as the best realization of the highly frustrated antiferromagnetic kagome lattice known so far. No order has been found at any temperatures despite its strong magnetic interactions. These results indicate that it is a promising candidate for a spin liquid state expected for $S = 1/2$ quantum spins on a kagome lattice [9]. A tremendous amount of theoretical and experimental reports have been published, yet many unanswered issues persist concerning the intrinsic ground state of this $S = 1/2$ kagome antiferromagnet [10].

On the other hand, the kagome lattice $\text{ZnCu}_3(\text{OH})_6\text{Cl}_2$ belongs to the atacamite family and can be obtained by selectively replacing 1/4 of Cu with Zn in its parent compounds of deformed pyrochlore lattice atacamite or clinoatacamite $\text{Cu}_2(\text{OH})_3\text{Cl}$ (or more properly expressed as $\text{Cu}_4(\text{OH})_6\text{Cl}_2$).

The pyrochlore lattice consists of alternatively stacked planes of triangular lattice and kagome lattice, wherein selective replacement was enabled due to the different chemical environment for the Cu in the triangular lattice and kagome lattice planes in $\text{Cu}_4(\text{OH})_6\text{Cl}_2$. The deformed pyrochlore lattice compounds of atacamite and clinoatacamite themselves were found to be geometrically frustrated systems showing a disordered ground state and order/spin liquid coexisting behaviors, respectively [11,12]. In principle, other kagome lattice compounds can be prepared from their parent compounds of transition metal hydroxyl salts $M_2(\text{OH})_3\text{Cl}$ ($M = \text{Ni}^{2+}, \text{Co}^{2+}, \text{Fe}^{2+}, \text{Mn}^{2+}$), which all showed features of frustrated magnetism [13–17], establishing a precious real material system ranging from the quantum limit to classical. Among them, the Ising-like $S = 3/2$ kagome antiferromagnet $\text{ZnCo}_3(\text{OD})_6\text{Cl}_2$ and $\text{MgCo}_3(\text{OH})_6\text{Cl}_2$ showed short-range correlations with persistent spin fluctuations in the vicinity of the ordered state below $T = 2.7$ K [18,19]. The $S = 2$ $\text{MgFe}_3(\text{OH})_6\text{Cl}_2$ behaved like a Heisenberg spin system showing a 120° nearest-neighbor long-range order (LRO) with negative spin chirality at $T_N = 9.9$ K [20]. In addition, the same method was shown applicable to synthesize $\text{MgMn}_3(\text{OH})_6\text{Cl}_2$, which showed an antiferromagneticlike transition. There envisaged a distinct tendency from spin liquid to LRO with increased magnetic moment. However, concerns remained whether the LRO is intrinsic for classical Heisenberg spin systems. Therefore, we were motivated to further explore the evolution of magnetism in the spin-5/2 system $\text{MgMn}_3(\text{OH})_6\text{Cl}_2$ —the end classical spin compound in the transition metal hydroxyl series.

*Corresponding author: zheng@cc.saga-u.ac.jp

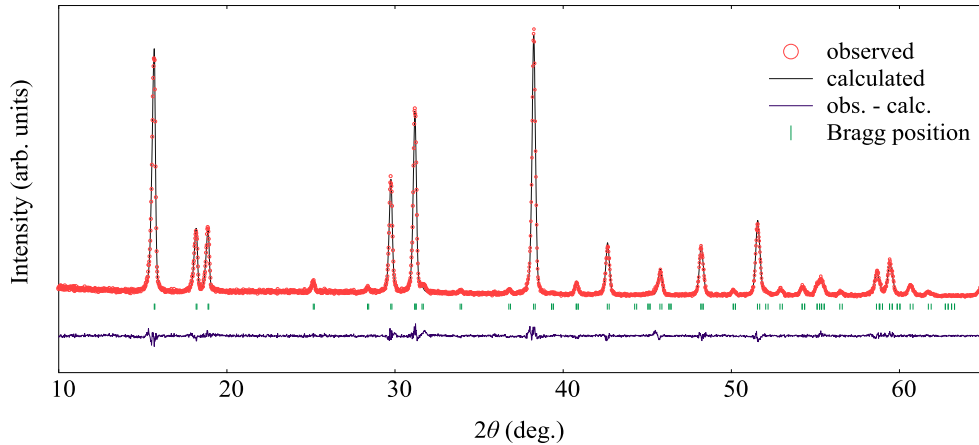


FIG. 1. X-ray powder-diffraction pattern (red circles) for kagome lattice compound $\text{Mg}_{1.55}\text{Mn}_{2.45}(\text{OH})_6\text{Cl}_2$ at room temperature and the result of Rietveld refinements showing the calculated (black solid line) pattern and the difference between the experimental and calculated data (thin violet solid line). The green bar represents the Bragg position of the present compound.

The $S = 5/2$ kagome antiferromagnet was realized in another material system of jarosite, i.e., potassium jarosite $\text{KFe}_3(\text{OH})_6(\text{SO}_4)_2$, plumbogjarosite $\text{Pb}_{0.5}\text{Fe}_3(\text{OH})_6(\text{SO}_4)_2$, and argentojarosite $\text{AgFe}_3(\text{OH})_6(\text{SO}_4)_2$, wherein a $q = 0$ LRO with positive spin chirality at a high T_N up to 65 K was reported [21–23]. The presence of nonmagnetic defects and weak ion anisotropy were tentatively supposed to explain the unexpected LRO [21,23]. Experimental evidences suggested an Ising nature for the jarosite compounds.

Till now, almost all theoretical studies predicted an extremely high degeneracy of the ground states for a classical spin kagome antiferromagnet. For instance, the first-neighbor Heisenberg antiferromagnet on the kagome lattice has an extensive degeneracy without long-range order even at $T = 0$ [24,25]. A second-neighbor Heisenberg coupling J_2 leads to a $q = 0$ Néel order for $J_2 > 0$ (antiferromagnetic interactions) or a $q = \sqrt{3} \times \sqrt{3}$ order for $J_2 < 0$ (ferromagnetic interactions) near $T = 0$ [26]. Extension of the $J_1 - J_2$ model to ferromagnetic nearest-neighbor coupling ($J_1 < 0$) leads to a Néel long-range order near $T = 0$ for $J_2 \geq -J_1/3$ with 12 noncoplanar sublattices and incommensurate noncoplanar structures for $J_2 < -J_1/3$ [27]. More recently, the interplay of dipolar interactions and geometrical frustration has been discussed and long-range ordering has been shown to be stabilized by consideration of both dipolar and nearest-neighbor interactions [28,29]. Conversely, the classical model for an Ising kagome antiferromagnet remains disordered even at $T = 0$ [30,31]. A more recent Monte Carlo simulation study has predicted long-range order for the classical dipolar Ising kagome antiferromagnet [32]. While the quantum fluctuations for a Heisenberg kagome antiferromagnet can lift the degeneracy and lead to order from disorder at $T = 0$ [33], they fail to induce magnetic order for the Ising model at any temperature [34,35]. Despite these advancements, it is clear that the nature of the classical low-temperature states for both Heisenberg and Ising kagome antiferromagnets remains largely unknown. Meanwhile, there is a much bigger discrepancy between theoretical prediction and experimental result for the classical kagome antiferromagnets as compared to the quantum spin

kagome system. Therefore, the ground state of the kagome antiferromagnet $\text{MgMn}_3(\text{OH})_6\text{Cl}_2$ is of considerable interest both as a quasiclassical kagome antiferromagnet as well as a reference system for the spin liquid kagome antiferromagnets $\text{ZnCu}_3(\text{OH})_6\text{Cl}_2/\text{MgCu}_3(\text{OH})_6\text{Cl}_2$.

II. EXPERIMENTAL PROCEDURES

For nonmagnetic ion substitution into $\text{Mn}_4(\text{OH})_6\text{Cl}_2$, Mg was found more effective than Zn, which may be accounted for by its smaller ion radius. Whitish polycrystalline powder of $\text{Mg}_x\text{Mn}_{4-x}(\text{OH})_6\text{Cl}_2$, with a nominal ideal chemical formula of $\text{MgMn}_3(\text{OH})_6\text{Cl}_2$, as synthesized using a solvothermal reaction of water-ethanol solutions of $\text{MgCl}_2 \cdot 6\text{H}_2\text{O}$, $\text{MnCl}_2 \cdot 4\text{H}_2\text{O}$, and NaOH in molar ratios of Mg/Mn = 0.5–3 at around 150–200 °C for 120 h in a nitrogen atmosphere [dried MgCl_2 and MnCl_2 , NaOD were used for $\text{Mg}_x\text{Mn}_{4-x}(\text{OD})_6\text{Cl}_2$]. The product was washed to remove unreacted MgCl_2 and NaCl using ethylene glycol and dried in vacuum (exposure to air or water containing oxygen would cause oxidation to change the powder to a brownish color on the surface). Since site mixing seemed inevitable as well known in herbertsmithite $\text{Mg}_x\text{Mn}_{4-x}(\text{OH})_6\text{Cl}_2$ with different ratios of Mg/Mn were prepared to assess the effect of nonmagnetic defects on the magnetism of $\text{MgMn}_3(\text{OH})_6\text{Cl}_2$. A powder x-ray diffraction (XRD) measurement was performed using an x-ray diffractometer ($\text{CuK}\alpha$), and analyzed using the Rietveld method with the computer program RIETAN-FP [36]. The DC susceptibility measurements were carried out using a commercial superconducting quantum interference device magnetometer (MPMS; Quantum Design). A neutron powder-diffraction experiment was performed on $\text{MgMn}_3(\text{OD})_6\text{Cl}_2$ using the superhigh resolution powder diffractometer (SuperHRPD) in the time of flight (TOF) mode at J-PARC, Japan. The TOF were analyzed using the Rietveld analysis software for J-PARC [37]. The collected neutron data were refined using the FULLPROF-suite software based on Rietveld refinement [38], assisted by the representation analysis program SARAh [39].

TABLE I. Structural information of $\text{Mg}_{1.55}\text{Mn}_{2.45}(\text{OH})_6\text{Cl}_2$ refined from x-ray powder diffraction at 300 K (site $9e$ and $3b$ correspond to the kagome plane site and triangular plane site, respectively).

Chemical formula		$\text{Mg}_{1.55}\text{Mn}_{2.45}(\text{OH})_6\text{Cl}_2$					
Cell setting		Rhombohedral					
Space group		$R\text{-}3m$ (No. 166)					
a (Å)		7.15420(4)					
c (Å)		14.80045(7)					
$\alpha = \beta = 90^\circ, \gamma = 120^\circ$							
$R_{\text{wp}}(S)$		9.6 (1.2)					
R_p		6.9					
Site	Sym	x	y	z	g	B	
Mg1	$9e$	$.2/m$	0.5	0	0	0.19(1)	1.125(8)
Mn1	$9e$	$.2/m$	0.5	0	0	0.81(1)	1.125(8)
Mg2	$3b$	$-3m$	0	0	0.5	0.98(1)	1.428(3)
Mn2	$3b$	$-3m$	0	0	0.5	0.02(1)	1.428(3)
Cl	$6c$	$3m$	0	0	0.2133(2)	1.0	1.975(2)
O	$18h$	$.m$	0.2015(3)	0.4030(6)	0.0730(2)	1.0	1.557(2)

III. RESULTS AND DISCUSSION

Analysis of the XRD pattern, as exemplified in Fig. 1 showed that the kagome-lattice compounds $\text{Mg}_x\text{Mn}_{4-x}(\text{OH})_6\text{Cl}_2$ were successfully synthesized by selectively replacing the Mn^{2+} ions in the triangular-lattice planes of its parent compound $\text{Mn}_2(\text{OH})_3\text{Cl}$. The parent compound $\text{Mn}_2(\text{OH})_3\text{Cl}$ crystallizes in orthorhombic structure with lattice constant $a = 6.49$ Å, $b = 7.11$ Å, and $c = 9.52$ Å in space group $Pnma$, No. 62 [17,40], whereas the $\text{Mg}_x\text{Mn}_{4-x}(\text{OH})_6\text{Cl}_2$ was found to crystallize in a rhombohedral structure with space group $R\text{-}3m$ (No. 166). The structure data on one sample of $\text{Mg}_{1.55}\text{Mn}_{2.45}(\text{OH})_6\text{Cl}_2$ are summarized in Table I and illustrated in Fig. 2(a). The triangular site (site $3b$ in the table) Mn ions were actually 98.0% replaced by Mg^{2+} ions; whereas 19.0% of the $9e$ kagome site Mn were also replaced. The 81% Mn^{2+} occupancy at the

kagome site is higher than the percolation threshold for kagome ($p_c^{\text{site}} = 65\%$) [41]. Since the nonmagnetic defects may be a crucial factor to influence the magnetism on the kagome lattice, we synthesized the compound using various conditions to produce various $\text{Mg}_x\text{Mn}_{4-x}(\text{OH})_6\text{Cl}_2$ around the nominal $\text{MgMn}_3(\text{OH})_6\text{Cl}_2$, which all crystallized in an equivalent structure as summarized in Table II. The present study revealed that Mg^{2+} ions prefer to occupy the octahedral triangular sites. For example, in the nominal formula of $\text{Mg}_{0.90}\text{Mn}_{3.10}(\text{OH})_6\text{Cl}_2$, 66% of the triangular Mn were replaced by Mg, but only 8% of the kagome Mn were replaced. However, more Mg entered the kagome sites when Mn is heavily substituted. This situation is similar to that occurring in herbertsmithite $\text{ZnCu}_3(\text{OH})_6\text{Cl}_2$, $(\text{Mg}/\text{Zn})\text{Co}_3(\text{OH})_6\text{Cl}_2$, and $\text{MgFe}_3(\text{OH})_6\text{Cl}_2$. Although an ideal perfect kagome lattice cannot be realized, we can get a plausible conclusion by investigating the magnetism

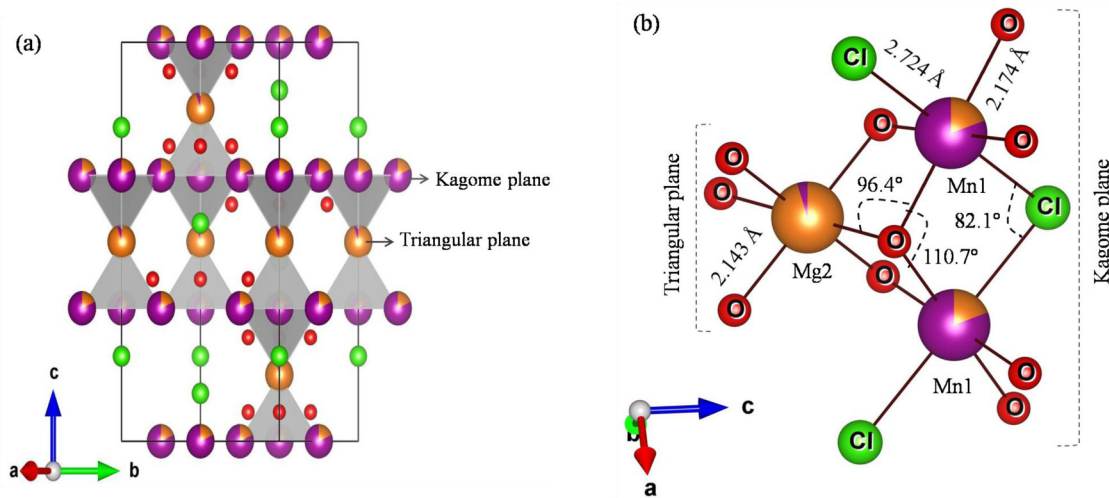


FIG. 2. (a) Crystal structure of $\text{Mg}_{1.55}\text{Mn}_{2.45}(\text{OH})_6\text{Cl}_2$ showing alternately stacked layers of the kagome and triangular lattice planes along the c -axis direction, wherein the yellow, violet, green, and red colored spheres represent Mg^{2+} , Mn^{2+} , Cl^- , and O^{2-} ion, respectively. (b) Local environment around the nonmagnetic Mg^{2+} ion (yellow sphere) at the triangular site and the magnetic Mn^{2+} ion (violet sphere) at the kagome site.

TABLE II. Summary of $\text{Mg}_x\text{Mn}_{4-x}(\text{OH})_6\text{Cl}_2$ compounds with varied total substitution rate x , substitution rate in kagome plane, and substitution rate in triangular plane.

Compound formula	Substitution rate x	Substitution rate in kagome plane	Substitution rate in triangular plane
$\text{Mg}_{0.90}\text{Mn}_{3.10}(\text{OH})_6\text{Cl}_2$	0.90	0.08(1)	0.66(1)
$\text{Mg}_{1.15}\text{Mn}_{2.85}(\text{OH})_6\text{Cl}_2$	1.15	0.10(2)	0.85(2)
$\text{Mg}_{1.27}\text{Mn}_{2.73}(\text{OH})_6\text{Cl}_2$	1.27	0.11(2)	0.94(1)
$\text{Mg}_{1.50}\text{Mn}_{2.50}(\text{OH})_6\text{Cl}_2$	1.50	0.18(2)	0.96(1)
$\text{Mg}_{1.55}\text{Mn}_{2.45}(\text{OH})_6\text{Cl}_2$	1.55	0.19(1)	0.98(1)
$\text{Mg}_{1.62}\text{Mn}_{2.38}(\text{OH})_6\text{Cl}_2$	1.62	0.21(3)	0.99(3)

evolution in the $\text{Mg}_x\text{Mn}_{4-x}(\text{OH})_6\text{Cl}_2$ samples with different degrees of substitution of the triangular lattice Mn and defects in the kagome lattice.

The local environments of $\text{Mg}_{1.55}\text{Mn}_{2.45}(\text{OH})_6\text{Cl}_2$ around the kagome and triangular sites are illustrate in Fig. 2(b). The Mn/Mg (Mn1) at kagome site is surrounded by four O^{2-} and two Cl^- ions, whereas Mg/Mn (Mg2) in the triangular site is surrounded by six O^{2-} ions in the octahedral environment. Therefore, selective replacement was enabled due to the different chemical environments for the Mn in the triangular lattice and kagome lattice planes. The Mn1-O, and Mn1-Cl bond length around the kagome site are 2.174 and 2.724 Å, respectively; whereas the Mg-O bond length around the triangular site is 2.143 Å. In the kagome plane, each Mn^{2+} ion is bridged with another Mn^{2+} ion via O, or Cl ions, with angles of $\angle\text{Mn1-O-Mn1} = 110.7^\circ$ and $\angle\text{Mn1-Cl-Mn1} = 82.1^\circ$. Analogous to the herbertsmithite $\text{ZnCu}_3(\text{OH})_6\text{Cl}_2$, superexchange interactions should occur via the Mn1-O-Mn1 bridge, with possible additional coupling via Mn1-Cl-Mn1. The kagome Mn1 and residual triangular Mn2 is double bridged via two Mn1-O-Mn2 bonds angled $\angle\text{Mn1-O-Mn2} = 96.4^\circ$. These kinds of double bridges were seen in antiferromagnetic CuOHCl , as well as in LiNiO_2 and NaNiO_2 [42–45].

The refined lattice constants in relation to the substitution rate x in $\text{Mg}_x\text{Mn}_{4-x}(\text{OH})_6\text{Cl}_2$ for $x = 0.9$ –1.62 are plotted in Fig. 3. More specifically, those in relation to the substitution rates in the triangular plane x_{tri} and kagome plane x_{kag} , respectively, in $\text{Mg}_{x_{\text{tri}}}\text{Mn}_{1-x_{\text{tri}}}\text{Mg}_{3x_{\text{kag}}}\text{Mn}_{3(1-x_{\text{kag}})}(\text{OH})_6\text{Cl}_2$ are presented. The tendency is well seen in relation to the x_{tri} . With substitution of Mn by smaller Mg, the c -axis length is slightly reduced till $x_{\text{tri}} \sim 0.85$. Meanwhile, the a -axis length, which depends on the ions in the kagome plane, remains almost unchanged. When x_{tri} exceeds 0.85, Mg also enters the kagome plane, thus effectively reducing the a -axis length. These consistent changes demonstrate the soundness of the structural analyses.

All $\text{Mg}_x\text{Mn}_{4-x}(\text{OH})_6\text{Cl}_2$ ($x = 0.9$ –1.62) samples showed similar magnetic behaviors with slightly different T_N values. The temperature dependence of DC susceptibility and inverse susceptibility of $\text{Mg}_{1.50}\text{Mn}_{2.50}(\text{OH})_6\text{Cl}_2$ is shown in Fig. 4. Antiferromagnetic transition at $T_N = 7.9$ K was observed, which was much enhanced than that in its parent compound $\text{Mn}_2(\text{OH})_3\text{Cl}$ of $T_{N1} = 3.4$ K and $T_{N2} = 2.7$ K [17]. The low-temperature upturn in the susceptibility, similarly observed for all samples studied, is similar to that observed in $\text{MgFe}_3(\text{OH})_6\text{Cl}_2$ [20], which is a common feature in geo-

metrically frustrated systems reflecting spin fluctuations. The small anomaly at ~ 40 K was suspected to be due to trace impurity of manganese oxides formed on the powder surface due to oxidation in air. Further measurements at zero-field cooled (ZFC) and field-cooled (FC) conditions confirmed that it agreed well with the $T_C = 40$ K ferromagnetic Mn_3O_4 [46–48]. Although glassiness was observed in the $x = 0$ compound $\text{Mn}_2(\text{OH})_3\text{Cl}$, notable glassiness was not recognized in $\text{Mg}_x\text{Mn}_{4-x}(\text{OH})_6\text{Cl}_2$ for $x = 0.9$ –1.62, except the ZFC/FC

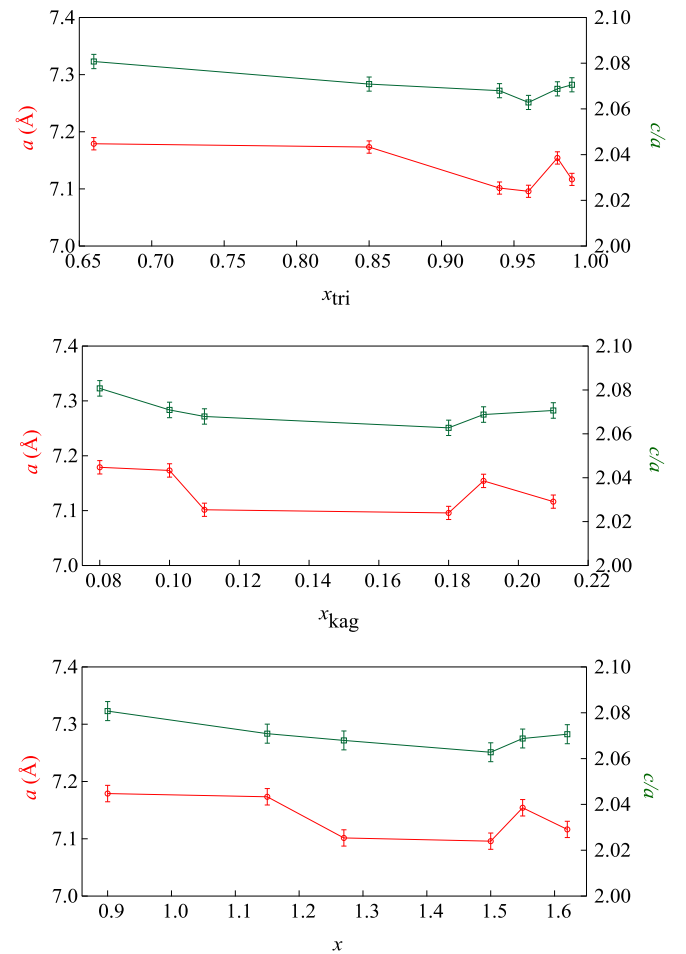


FIG. 3. Changes of lattice constants related to Mg substitution ratios of the total substitution x , kagome plane substitution x_{kag} , and triangular plane substitution x_{tri} in $\text{Mg}_x\text{Mn}_{4-x}(\text{OH})_6\text{Cl}_2$.

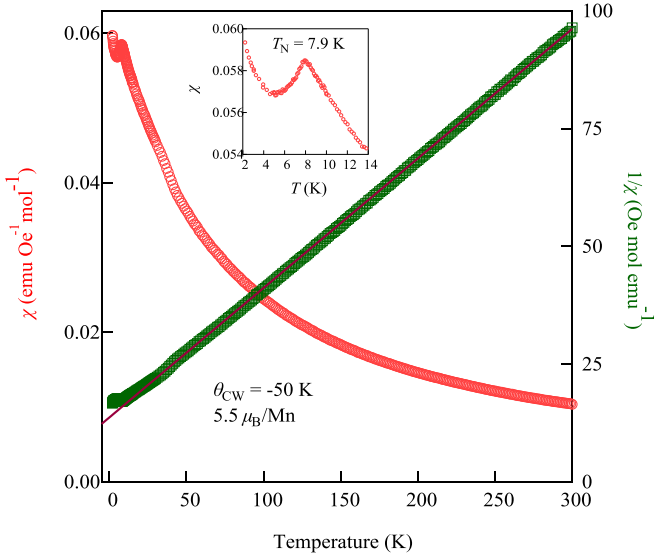


FIG. 4. Temperature dependences of dc susceptibilities χ (left axis, red open circles), and inverse susceptibilities $1/\chi$ (right axis, open green squares) per mol Mn for $\text{Mg}_{1.5}\text{Mn}_{2.5}(\text{OH})_6\text{Cl}_2$ measured at $H = 10$ kOe. The solid line obeys the Curie-Weiss law, with a Weiss temperature θ_{CW} of approximately -50 K. The inset plot is an enlarged view of the χ - T showing the antiferromagnetic transition.

diverging starting from 40 K due to suspected partial oxidation to ferromagnetic Mn_3O_4 .

The Curie-Weiss temperature was estimated to be $\vartheta_W = -50$ K, showing a much reduced geometrical frustration index of $f = \vartheta_W/T_N \sim 6.3$, as compared to the $f = 17$ in $\text{Mn}_2(\text{OH})_3\text{Cl}$. Similar tendency of reduced frustration from the pyrochlore parent compounds to kagome compounds was seen in $\text{MgFe}_3(\text{OH})_6\text{Cl}_2$ [20]. The effective magnetic moment per Mn^{2+} ion was estimated to be $5.5 \mu_B$, which is slightly smaller than the spin only moment $\mu_{\text{mag}}^{\text{calc.}} = g\mu_B\sqrt{S(S+1)} = 5.92 \mu_B$ for $S = \frac{5}{2}\text{Mn}^{2+}$. This value is close to the experimentally reported $\mu_{\text{mag}}^{\text{obs.}} = 5.6\text{--}6.1 \mu_B$ for normal type Mn^{2+} ,

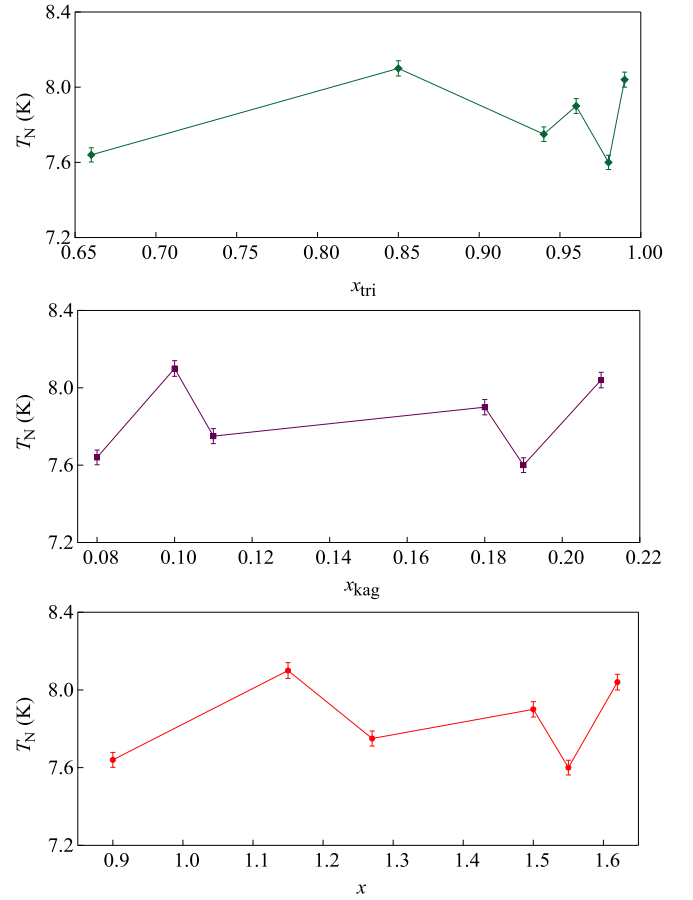


FIG. 5. Changes in transition temperature T_N related to Mg substitution ratios of the total substitution x , kagome plane substitution x_{kag} , and triangular plane substitution x_{tri} in $\text{Mg}_x\text{Mn}_{4-x}(\text{OH})_6\text{Cl}_2$ ($x = 0.9\text{--}1.62$).

wherein the orbital contribution to the spin-only values for ions of the first transition period lead to somewhat smaller or larger effective magnetic moments. As shown in Fig. 5 in the

TABLE III. Structural information of kagome lattice compound $\text{Mg}_{1.34}\text{Mn}_{2.67}(\text{OD})_6\text{Cl}_2$ refined from neutron powder diffraction at 20 K (site $9e$ and $3b$ correspond to the kagome plane site and triangular plane site, respectively).

Chemical formula		$\text{Mg}_{1.34}\text{Mn}_{2.67}(\text{OD})_6\text{Cl}_2$					
Cell setting		Rhombohedral					
Space group		$R\bar{3}m$ (No. 166)					
a (Å)		7.06973(4)					
c (Å)		14.59632(2)					
$\alpha = \beta = 90^\circ, \gamma = 120^\circ$							
$R_{\text{wp}}(\%)$		4.9					
$R_{\text{p}}(\%)$		3.7					
Site	Sym	x	y	z	g	B	
Mg1	$9e$	$.2/m$	0.5	0	0	0.15(3)	0.6342(2)
Mn1	$9e$	$.2/m$	0.5	0	0	0.85(3)	0.6342(2)
Mg2	$3b$	$\bar{3}m$	0	0	0.5	0.89(7)	0.9592(7)
Mn2	$3b$	$\bar{3}m$	0	0	0.5	0.11(7)	0.9592(7)
Cl	$6c$	$3m$	0	0	0.2180(3)	1.0	1.1016(4)
O	$18h$	$.m$	0.2079(1)	0.4158(2)	0.0719(1)	1.0	1.2140(4)
D	$18h$	$.m$	0.1424(2)	0.2848(4)	0.0975(1)	1.0	1.1413(4)

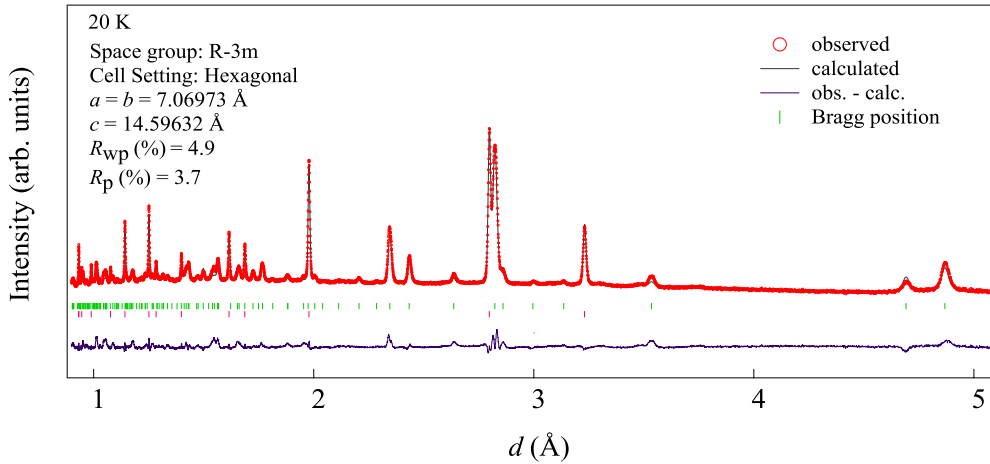


FIG. 6. Neutron powder diffraction pattern (red circles) for $\text{MgMn}_3(\text{OD})_6\text{Cl}_2$ at 20 K and the result of Rietveld refinements showing the calculated (black solid line) pattern and the difference between the experimental and calculated data (thin violet solid line). The vertical green bars represent the Bragg positions of the present compound. The specimen contained some accidentally included NaCl due to insufficient washing during preparation, as indicated by the violet bars beneath the Bragg positions of $\text{MgMn}_3(\text{OD})_6\text{Cl}_2$.

substitution range the T_N was enhanced by more completely replacing Mn in the triangular plane with Mg. Nevertheless, the T_N only slightly varied between 7.6–8.0 K, showing that the nonmagnetic defects in the kagome site did not have a substantial effect on the ordering.

The neutron powder diffraction data measured at 20 K for $\text{Mg}_{1.34}\text{Mn}_{2.67}(\text{OD})_6\text{Cl}_2$ and the Rietveld refinement results are presented in Fig. 6 and Table III wherein the atomic position of D was added as compared to Table I for $\text{Mg}_x\text{Mn}_{4-x}(\text{OH})_6\text{Cl}_2$. Neutron powder diffraction experiments were also performed at various temperatures to see the temperature change of the lattice constants. No structural transition was observed except a prominent increase of the lattice constant ratio c/a with decreasing temperature as shown in Fig. 7.

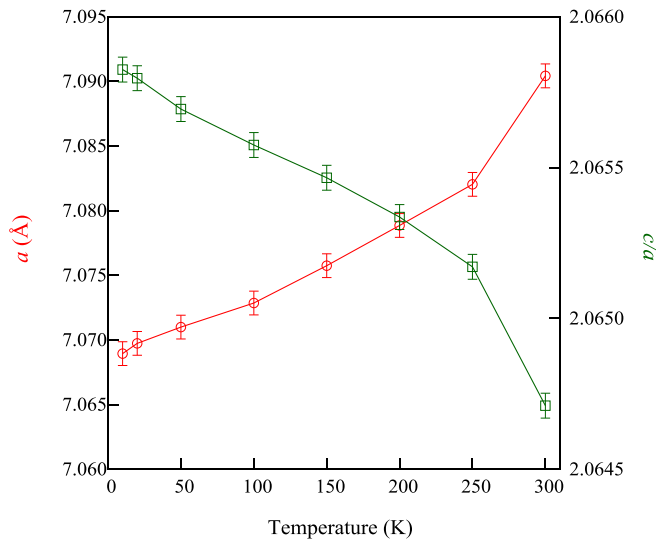


FIG. 7. Temperature dependence of lattice constant a (left axis, filled red circles) and the ratio of c/a for $\text{MgMn}_3(\text{OD})_6\text{Cl}_2$ (right axis, filled green squares).

Neutron diffraction patterns at 20 and 2.7 K, and their difference, are plotted in Fig. 8. Long-range antiferromagnetic order below 8 K developed in $\text{Mg}_{1.34}\text{Mn}_{2.67}(\text{OD})_6\text{Cl}_2$ and the difference curve clearly demonstrates magnetic reflections at $(0, 1, \frac{1}{2})$, $(1, 0, \frac{5}{2})$, and $(1, -1, \frac{7}{2})$ Bragg position with propagation vector $\mathbf{k} = (0, 0, \frac{3}{2})$. The critical exponent β was estimated to be $\beta = 0.35(3)$ using the relation, $I = I_0(1 - T/T_N)^{2\beta}$ by fitting the temperature dependence of integrated intensities of the $(0, 1, \frac{1}{2})$ reflection, wherein $T_N = 7.5(1)$ K. This value is close to the $\beta = 0.355(17)$ in its sister compound of $S = 2$ Heisenberg spin $\text{MgFe}_3(\text{OH})_6\text{Cl}_2$ [20]. The theoretical critical exponents for several spin models are $\beta = 0.253$ for $\text{SO}(2) \times Z_2$ in 3D, $\beta = 0.125$ for a 2D Ising system, and $\beta = 0.365$ for a 3D Heisenberg system [49–52]. The spin model of $\text{SO}(2) \times Z_2$ corresponds to the frustrated XY triangular lattice antiferromagnet, whereas the other spin models are nonfrustrated systems. The critical exponents depend on symmetry of interaction, the dimensionality of the system, and the existence of frustration. From the comparison of the present experimental critical exponent to the theoretical values taking into consideration the factor of frustration, the present system can be viewed a Heisenberg spin system. It is interesting to compare this result to the small β of 0.19(1) in the $S = 5/2$ kagome antiferromagnet $\text{KFe}_3(\text{OH})_6(\text{SO}_4)_2$, wherein two-dimensional Ising symmetry due to the anisotropy was reported [53]. Therefore, unlike the present Heisenberg spin system of $S = 5/2$ $\text{MgMn}_3(\text{OH})_6\text{Cl}_2$, the $S = 5/2$ jarosites should be rather viewed as an Ising system.

All symmetrically allowed magnetic structures were derived using the irreducible representation program SARAH. The possible magnetic structures for magnetic propagation vector $\mathbf{k} = (0, 0, 3/2)$ in the $R-3m$ (No. 166) space group were found as $\Gamma_{\text{mag}} = \Gamma_1(A_{1g}) + 2\Gamma_3(A_{2g}) + 6\Gamma_5(E_g)$, wherein Γ_i indicates irreducible representations and there are one basis vector for Γ_1 two basis vectors for Γ_3 , and six basis vectors for Γ_5 . Fifteen magnetic models with the combination of two basis vector given by ${}_6C_2 = 15$ were tested for Γ_5 irreducible

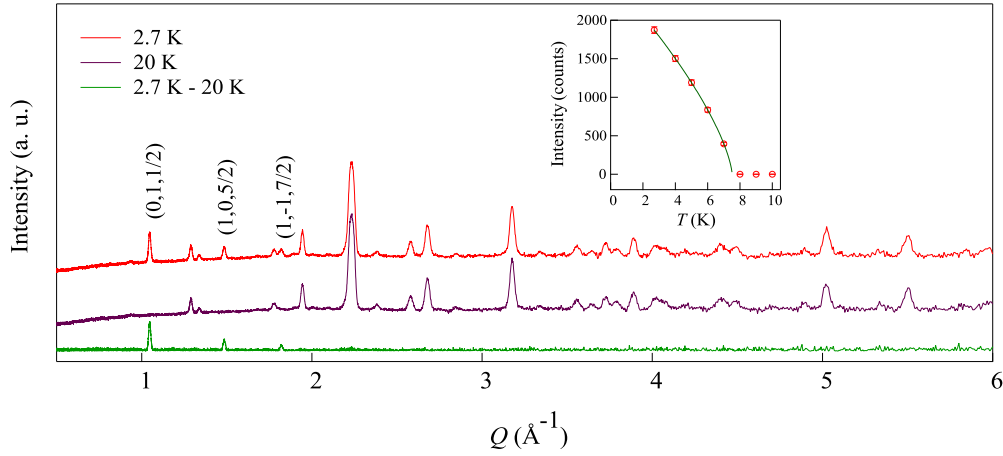


FIG. 8. Neutron powder-diffraction patterns of $\text{Mg}_{1.34}\text{Mn}_{2.67}(\text{OD})_6\text{Cl}_2$ at 2.7 and 20 K. The inset plot depicts the integrated intensity change of the $(0, 1, \frac{1}{2})$ magnetic peak with respect to temperature for $\text{Mg}_{1.34}\text{Mn}_{2.67}(\text{OD})_6\text{Cl}_2$. The solid line is the power-law fit $I = I_0(1 - T/T_N)^{2\beta}$.

representation. Out of 15 magnetic models for Γ_5 , only $\Gamma_5(\varphi_6 + \varphi_9)$ has the lowest magnetic reliable factor of $R_{\text{mag}} = 29.8$. However, as shown in Fig. 9 the fitting is inconsistent to the experimental data and it unreasonably produced different magnetic moments of 4.5, 3.6, and $0.88 \mu_B$ for three crystallographically equivalent Mn ions in the kagome plane. The $\Gamma_3(\varphi_2 + \varphi_3)$ produced a very poor fitting ($R_{\text{mag}} = 53.2$) with equivalent magnetic moments of $4.5 \mu_B$ for the three Mn ions. The previously reported chirality -1 structures as described for $\text{MgFe}_3(\text{OD})_6\text{Cl}_2$ [20] gave even poorer fitting. The best fitting was obtained with the irreducible representation $\Gamma_1(\varphi_1)$

with a small $R_{\text{mag}} = 12.7$ and an equivalent $4.7 \mu_B$ for the three Mn ions in the kagome lattice plane. Apparently, the $\Gamma_1(\varphi_1)$ with a 120° nearest-neighbor spin ordering confined on the kagome lattice plane, as visualized in Fig. 10 should represent the spin structure in $\text{Mg}_{1.34}\text{Mn}_{2.67}(\text{OD})_6\text{Cl}_2$. According to the definition of spin chirality [50], which is an important concept for kagome antiferromagnets, the spin arrangement of $\Gamma_1(\varphi_1)$ has spin chirality of $+1$ (clockwise).

The 120° spin ordering at a relatively high $T_N \sim 8$ K in $\text{Mg}_{1.34}\text{Mn}_{2.67}(\text{OD})_6\text{Cl}_2$ is similar to that in its sister compound $S = 2$ $\text{MgFe}_3(\text{OD})_6\text{Cl}_2$ at $T_N = 9.9$ K, although the latter has an opposite spin vector chirality -1 . Long-range ordering at such high transition temperatures distinctly differ from those predicted for classical Heisenberg models by most theoretical investigations. Although Mg and Mn intermixing exists in the present $\text{Mg}_x\text{Mn}_{4-x}(\text{OH})_6\text{Cl}_2$ system, we tend to conclude that long-range ordering is intrinsic for the nominal $\text{MgMn}_3(\text{OH})_6\text{Cl}_2$ for reasons described below. First, all $\text{Mg}_x\text{Mn}_{4-x}(\text{OH})_6\text{Cl}_2$ ($x = 0.9-1.62$) samples with different Mg/Mn site intermixing showed similar magnetism, suggesting that the defects did not affect the ordering in $\text{MgMn}_3(\text{OH})_6\text{Cl}_2$. Second, the ordering in the present

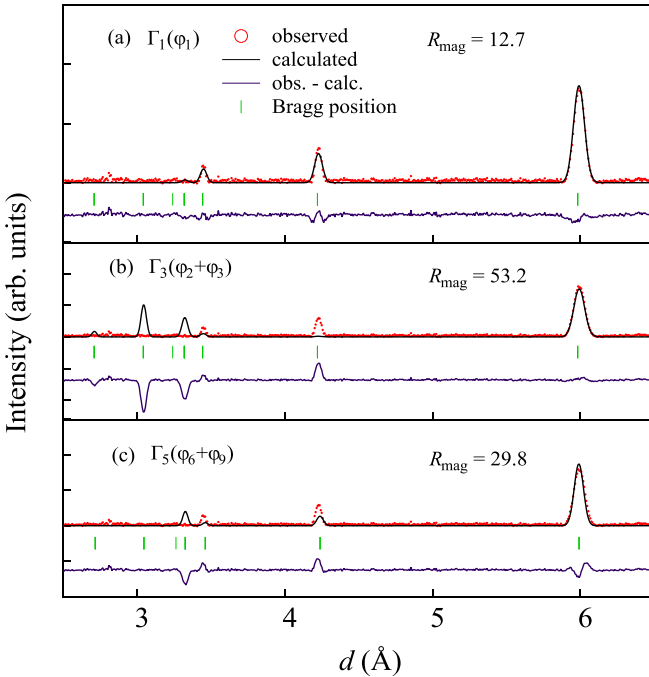


FIG. 9. Observed magnetic reflections (red circles), calculated intensities (black solid line) and the difference between the experimental and calculated data (blue solid line) for: (a) $\Gamma_1(\varphi_1)$, (b) $\Gamma_3(\varphi_2 + \varphi_3)$, and (c) $\Gamma_5(\varphi_6 + \varphi_9)$ in $\text{Mg}_{1.34}\text{Mn}_{2.67}(\text{OD})_6\text{Cl}_2$. The green bars represent the magnetic Bragg-peak positions.

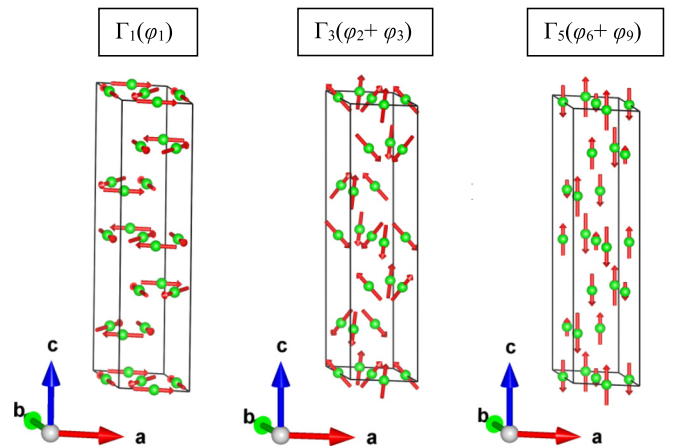


FIG. 10. Illustration of the magnetic structures of $\Gamma_1(\varphi_1)$, $\Gamma_3(\varphi_2 + \varphi_3)$, and $\Gamma_5(\varphi_6 + \varphi_9)$, respectively, for $\text{MgMn}_3(\text{OD})_6\text{Cl}_2$.

Heisenberg spin system $\text{Mg}_x\text{Mn}_{4-x}(\text{OH})_6\text{Cl}_2$ is strikingly different from the $S = 3/2$ Ising kagome antiferromagnets $\text{ZnCo}_3(\text{OH})_6\text{Cl}_2$ and $\text{MgCo}_3(\text{OH})_6\text{Cl}_2$, which have similar intermixing patterns but show partial spin liquid magnetism [18,19]. All of these results are consistent, therefore they are considered to support the intrinsic nature of the magnetic ordering in $\text{MgMn}_3(\text{OH})_6\text{Cl}_2$.

For a classical Heisenberg kagome antiferromagnet, most theoretical works predict a large ground state degeneracy or particular spin arrangements near $T = 0$, as described in the Introduction. The Dzyaloshinskii-Moriya (DM) interaction may lead to ordering with the $q = 0$ phase with the all-in all-out structure [54], which was previously proposed to account for the unexpected LRO in jarosites. Both planar and weak-ferromagnetic (along the axis perpendicular to the kagome plane) structures are obtained theoretically, which indeed agree with the experimentally observed results in jarosites. However, the Mn spin anisotropy in the present system appeared small. In addition, the magnetization of the samples did not show a DM-type weak-ferromagnetic property for $T < T_N$. Therefore, that kind of DM effect is considered to be absent. The high value of $T_N \sim 8$ K also appears too high to be accounted for by the order from disorder theories [28,33]. Besides, these models predicted tripled-unit-cell spin structures, which are different from that in $\text{Mg}_x\text{Mn}_{4-x}(\text{OH})_6\text{Cl}_2$.

It is interesting to compare the present regular kagome lattice system to the so-called kagome–triangular (KT) lattice of layered fluoride $\text{NaBa}_2\text{Mn}_3\text{F}_{11}$ [55]. In the latter, a kagome-type array of regular triangles composed of Mn^{2+} ions (spin 5/2) deforms much so as to generate a large next-nearest-neighbor interaction J_2 in addition to the nearest-neighbor interaction J_1 . This KT lattice compound showed a long-range order at 2.0 K, which is shown to be in good consistency with the unique noncoplanar magnetic orders predicted by the extended $J_1 - J_2$ model [27]. Indeed, the critical role of the next-nearest-neighbor interaction in inducing magnetic order in this kind of KT lattices has been also demonstrated in a triangular spin tube material CsCrF_4 , wherein ferromagnetic kagome bond, single-ion anisotropy, and DM interaction play key roles in the selection of the ground state [56].

Of the related theoretical models, the dipolar + Heisenberg interactions model proposed by Maksymenko *et al.* predicted a three-sublattice long-range order with coplanar 120° spin structure [29], which might be comparable to the present real system. The main exchange interaction J_e can be estimated approximately to be $J_e = -2.14$ K from the Curie-Weiss temperature θ_w using the mean-field theory by $J_e = \frac{3k_B\theta_w}{2zJ(J+1)}$, where z is the number of nearest neighbors. The dipolar interaction energy D is estimated to be 0.46 K for the Mn^{2+} spin using the relation $D = \frac{\mu_0 \mu^2}{4\pi R_{mn}^3}$, where $R_{mn} = 0.358$ nm.

The long-range order in the present $\text{Mg}_x\text{Mn}_{4-x}(\text{OH})_6\text{Cl}_2$ compounds with $D/J_e \sim 0.21$ may be qualitatively explained by the dipolar+Heisenberg interactions model. However, the high T_N near 8 K seems not be readily explainable. Most probably, dipolar+multiple Heisenberg interactions, including some interkagome-plane couplings, would better describe the magnetic order in $\text{MgMn}_3(\text{OH})_6\text{Cl}_2$. Especially, both $\text{MgFe}_3(\text{OH})_6\text{Cl}_2$ of spin chirality -1 and $\text{MgMn}_3(\text{OH})_6\text{Cl}_2$ of spin chirality $+1$ have an ordering wave vector $\mathbf{k} = (0, 0, \frac{3}{2})$, suggesting weak interplane superexchange interactions.

IV. CONCLUSIONS

In summary, an $S = 5/2$ classical Heisenberg kagome antiferromagnet $\text{Mg}_x\text{Mn}_{4-x}(\text{OH})_6\text{Cl}_2$, with a nominal ideal chemical formula of $\text{MgMn}_3(\text{OH})_6\text{Cl}_2$, has successfully synthesized. This kagome lattice compound crystallizes in rhombohedral structure with space group $R\bar{3}m$, in a similar crystal structure to the much-researched quantum spin liquid candidate herbertsmithite $\text{ZnCu}_3(\text{OH})_6\text{Cl}_2$. Relative to its parent compound of deformed pyrochlore $\text{Mn}_2(\text{OH})_3\text{Cl}$, magnetic frustration was significantly reduced, as demonstrated by the significant increase from $T_{N1} = 3.4$ K and $T_{N2} = 2.7$ K in $\text{Mn}_2(\text{OH})_3\text{Cl}$ to $T_N = 8.0$ K in $\text{MgMn}_3(\text{OH})_6\text{Cl}_2$. A long-range coplanar magnetic order developed below approximately 8 K in $\text{Mg}_{1.34}\text{Mn}_{2.67}(\text{OH})_6\text{Cl}_2$, which is strikingly different from its Cu variant of the quantum Heisenberg antiferromagnet $\text{ZnCu}_3(\text{OH})_6\text{Cl}_2$ in the same material series of magnetic transition metal hydroxyhalogenides. Recently, Merino *et al.* [57] reported theoretically rapid diminishing of quantum fluctuation with increasing the spin moment for honeycomb lattice. Our experimental verification of the magnetic ordering of $S = 5/2$ Heisenberg spin on a regular kagome lattice, and the previously reported $S = 2$ Heisenberg kagome antiferromagnet $\text{MgFe}_3(\text{OH})_6\text{Cl}_2$, provides simple real systems for further theoretical and experimental studies on classical kagome antiferromagnets.

ACKNOWLEDGMENTS

This research is supported by the Grant-in-Aid for Scientific Research (A) (Grant No. 19H00835) from the Japan Society for the Promotion of Science (JSPS). We acknowledge the financial support of Bangabandhu Science and Technology Fellowship Trust, Ministry of Science and Technology, Government of the People's Republic of Bangladesh to one of the authors as a scholarship to carry out their doctoral study in Saga University, Japan. The neutron diffraction experiment at the Materials and Life Science Experimental Facility of the J-PARC was performed under a user program (Proposal No. 2018A0102). T. Yuasa participated in the neutron diffraction experiment.

- [1] *Frustrated Spin Systems*, edited by H. T. Diep (World Scientific, Singapore, 2013).
- [2] Y. Zhou, K. Kanoda, and T.-K. Ng, *Rev. Mod. Phys.* **89**, 025003 (2017).
- [3] K. Ohgushi, S. Murakami, and N. Nagaosa, *Phys. Rev. B* **62**, R6065 (2000).

- [4] I. I. Mazin, *Nat. Commun.* **5**, 4261 (2014).
- [5] R. Chisnell, J. S. Helton, D. E. Freedman, D. K. Singh, R. I. Bewley, D. G. Nocera, and Y. S. Lee, *Phys. Rev. Lett.* **115**, 147201 (2015).
- [6] G. Xu, B. Lian, and S.-C. Zhang, *Phys. Rev. Lett.* **115**, 186802 (2015).

- [7] W. Zhu, S.-S. Gong, T.-S. Zeng, L. Fu, and D. N. Sheng, *Phys. Rev. Lett.* **117**, 096402 (2016).
- [8] J.-X. Yin, S. S. Zhang, H. Li, K. Jiang, G. Chang, B. Zhang, B. Lian, C. Xiang, I. Belopolski, H. Zheng, T. A. Cochran, S.-Y. Xu, G. Bian, K. Liu, T.-R. Chang, H. Lin, Z.-Y. Lu, Z. Wang, S. Jia, W. Wang, and M. Z. Hasan, *Nature (London)* **562**, 91 (2018).
- [9] P. Mendels, F. Bert, M. A. de Vries, A. Olariu, A. Harrison, F. Duc, J. C. Trombe, J. S. Lord, A. Amato, and C. Baines, *Phys. Rev. Lett.* **98**, 077204 (2007); P. Mendels and F. Bert, *C. R. Phys.* **17**, 455 (2016).
- [10] M. R. Norman, *Rev. Mod. Phys.* **88**, 041002 (2016).
- [11] X. G. Zheng, T. Mori, K. Nishiyama, W. Higemoto, H. Yamada, K. Nishikubo, and C. N. Xu, *Phys. Rev. B* **71**, 174404 (2005).
- [12] X. G. Zheng, T. Kawae, Y. Kashitani, C. S. Li, N. Tateiwa, K. Takeda, H. Yamada, C. N. Xu, and Y. Ren, *Phys. Rev. B* **71**, 052409 (2005); X. G. Zheng, H. Kubozono, K. Nishiyama, W. Higemoto, T. Kawae, A. Koda, and C. N. Xu, *Phys. Rev. Lett.* **95**, 057201 (2005).
- [13] X. G. Zheng, M. Hagihala, K. Nishiyama, and T. Kawae, *Physica B* **404**, 677 (2009).
- [14] X. G. Zheng, T. Kawae, H. Yamada, K. Nishiyama, and C. N. Xu, *Phys. Rev. Lett.* **97**, 247204 (2006).
- [15] M. Hagihala, X. G. Zheng, T. Kawae, and T. J. Sato, *Phys. Rev. B* **82**, 214424 (2010).
- [16] M. Fujihala, M. Hagihala, X. G. Zheng, and T. Kawae, *Phys. Rev. B* **82**, 024425 (2010).
- [17] M. Hagihala, X. G. Zheng, T. Toriyi, and T. Kawae, *J. Phys.: Condens. Matter* **19**, 145281 (2007).
- [18] M. Fujihala, X. G. Zheng, Y. Oohara, H. Morodomi, T. Kawae, A. Matsuo, and K. Kindo, *Phys. Rev. B* **85**, 012402 (2012).
- [19] S. E. Dissanayake, C. Chan, S. Ji, J. Lee, Y. Qiu, K. C. Rule, B. Lake, M. Green, M. Hagihala, X. G. Zheng, T. K. Ng, and S. H. Lee, *Phys. Rev. B* **85**, 174435 (2012).
- [20] M. Fujihala, X. G. Zheng, S. Lee, T. Kamiyama, A. Matsuo, K. Kindo, and T. Kawae, *Phys. Rev. B* **96**, 144111 (2017).
- [21] A. S. Will, A. Harrison, S. A. M. Mentink, T. E. Mason, and Z. Tun, *Europhys. Lett.* **42**, 325 (1998).
- [22] A. S. Wills, A. Harrison, C. Ritter, and R. I. Smith, *Phys. Rev. B* **61**, 6156 (2000).
- [23] T. Inami, M. Nishiyama, S. Maegawa, and Y. Oka, *Phys. Rev. B* **61**, 12181 (2000).
- [24] J. T. Chalker, P. C. W. Holdsworth, and E. F. Shender, *Phys. Rev. Lett.* **68**, 855 (1992).
- [25] R. Moessner and J. T. Chalker, *Phys. Rev. B* **58**, 12049 (1998).
- [26] A. B. Harris, C. Kallin, and A. J. Berlinsky, *Phys. Rev. B* **45**, 2899 (1992).
- [27] J.-C. Domenge, P. Sindzingre, C. Lhuillier, and L. Pierre, *Phys. Rev. B* **72**, 024433 (2005).
- [28] G.-W. Chern and R. Moessner, *Phys. Rev. Lett.* **110**, 077201 (2013).
- [29] M. Maksymenko, V. R. Chandra, and R. Moessner, *Phys. Rev. B* **91**, 184407 (2015).
- [30] K. Kano and S. Nava, *Prog. In Theor. Phys.* **10**, 158 (1953).
- [31] D. A. Huse and A. D. Rutenberg, *Phys. Rev. B* **45**, 7536(R) (1992).
- [32] I. A. Chioar, N. Rougemaille, and B. Canals, *Phys. Rev. B* **93**, 214410 (2016).
- [33] A. Chubukov, *Phys. Rev. Lett.* **69**, 832 (1992).
- [34] R. Moessner, S. L. Sondhi, and P. Chandra, *Phys. Rev. Lett.* **84**, 4457 (2000).
- [35] R. Moessner and S. L. Sondhi, *Phys. Rev. B* **63**, 224401 (2001).
- [36] F. Izumi and K. Momma, *Solid State Phenom.* **130**, 15 (2007).
- [37] R. Oishi, M. Yonemura, Y. Nishimaki, S. Toriia, Hoshikawa, T. Ishigaki, T. Morishima, K. Mori, and T. Kamiyama, *Nucl. Instrum. Methods Phys. Res. Sect. A* **600**, 94 (2009).
- [38] J. Rodriguez-Carvajal, *Physica B (Amsterdam)* **192**, 55 (1993).
- [39] A. S. Wills, *Physica B* **276–278**, 680 (2000).
- [40] K. Zenmyo, H. Kubo, M. Tokita, T. Hamasaki, M. Hagihala, and X. G. Zheng, *J. Phys. Soc. Jpn.* **80**, 024704 (2011).
- [41] X. Feng, Y. Deng, and H. W. J. Blöte, *Phys. Rev. E* **78**, 031136 (2008).
- [42] X.-G. Zheng, I. Yamauchi, S. Kitajima, M. Fujihala, M. Maki, S. Lee, M. Hagihala, S. Torii, T. Kamiyama, and T. Kawae, *Phys. Rev. Mater.* **2**, 104401 (2018).
- [43] L. F. Feiner, A. M. Oles, and J. Zaanen, *Phys. Rev. Lett.* **78**, 2799 (1997).
- [44] F. Reynaud, D. Mertz, F. Celestini, J.-M. Debierre, A. M. Ghorayeb, P. Simon, A. Stepanov, J. Voiron, and C. Delmas, *Phys. Rev. Lett.* **86**, 3638 (2001).
- [45] S. de Brion, M. D. Nunez-Regueiro, and G. Chouteau, in *Frontiers in Magnetic Materials*, edited by A. V. Narlikar (Springer, Berlin, 2005).
- [46] X. Sun, E. Feng, Y. Su, K. Nemkovski, O. Petracic, and T. Brückel, *J. Phys.: Conf. Ser.* **862**, 012027 (2017).
- [47] E. Winkler, J. P. Sinnecker, M. A. Novak, and R. D. Zysler, *J. Nanoparticle Res.* **13**, 5653 (2011).
- [48] B. Boucher, R. Buhl, and M. Perrin, *J. Appl. Phys.* **42**, 1615 (1971).
- [49] H. Kawamura, *J. Phys. Soc. Jpn.* **61**, 1299 (1992).
- [50] H. Kawamura and S. Miyashita, *J. Phys. Soc. Jpn.* **53**, 4138 (1984).
- [51] J. C. LeGuillou and J. Zinn-Justin, *Phys. Rev. B* **21**, 3976 (1980).
- [52] J. C. LeGuillou and J. Zinn-Justin, *J. Phys.* **50**, 1365 (1989).
- [53] M. Nishiyama, S. Maegawa, T. Inami, and Y. Oka, *Phys. Rev. B* **67**, 224435 (2003).
- [54] M. Elhajal, B. Canals, and C. Lacroix, *Phys. Rev. B* **66**, 014422 (2002).
- [55] H. Ishikawa, T. Okubo, Y. Okamoto, and Z. Hiroi, *J. Phys. Soc. Jpn* **83**, 043703 (2014).
- [56] M. Hagihala, S. Hayashida, M. Avdeev, H. Manaka, H. Kikuchi, and T. Masuda, *npj Quantum Mater.* **4**, 14 (2019).
- [57] J. Merino and A. Ralko, *Phys. Rev. B* **97**, 205112 (2018).